Appl Phys B (2010) 101: 631–638
DOI 10.1007/s00340-010-4199-z

Applied Physics B
Lasers and Optics

Infrared emissions, visible up-conversion, thermoluminescence and defect centres in $Er_3Al_5O_{12}$ phosphor obtained by solution combustion reaction

V. Singh · V.K. Rai · S. Watanabe · T.K. Gundu Rao · I. Ledoux-Rak · H.-Y. Kwak

Received: 12 November 2009 / Revised version: 1 July 2010 / Published online: 15 September 2010

Abstract The $Er_3Al_5O_{12}$ phosphor powders were prepared using the solution combustion method. Formation and homogeneity of the $Er_3Al_5O_{12}$ phosphor powders have been verified by X-ray diffraction and energy-dispersive X-ray analysis respectively. The frequency up-conversion from $Er_3Al_5O_{12}$ phosphor powder corresponding to the $^2H_{9/2} \rightarrow {}^4I_{15/2}$, $^2H_{11/2} \rightarrow {}^4I_{15/2}$, $^4S_{3/2} \rightarrow {}^4I_{15/2}$, $^4F_{9/2} \rightarrow {}^4I_{15/2}$ and the infrared emission (IR) due to the $^4I_{13/2} \rightarrow {}^4I_{15/2}$ transitions lying at ∼410, ∼524, ∼556, 645–680 nm and at ∼1.53 μm respectively upon excitation with a Ti-Sapphire pulsed/CW laser have been reported. The mechanism responsible for the frequency up-conversion and IR emission is discussed in detail. Defect centres induced by radiation were studied using the techniques of thermoluminescence and electron spin resonance. A single glow peak at 430°C is observed and the thermoluminescence results show the presence of a defect center which decays at high temperature. Electron spin resonance studies indicate a center characterized by a g-factor equal to 2.0056 and it is observed that this center is not related to the thermoluminescence peak. A negligibly small concentration of cation and anion vacancies appears to be present in the phosphor in accordance with the earlier theoretical predictions.

V. Singh (✉) · H.-Y. Kwak
Mechanical Engineering Department, Chung-Ang University, Seoul 156-756, Korea
e-mail: vijayjiin2006@yahoo.com

H.-Y. Kwak (✉)
e-mail: kwakh@cau.ac.kr

V.K. Rai
Department of Applied Physics, Indian School of Mines, Dhanbad 826004, India

S. Watanabe · T.K. Gundu Rao
Institute of Physics, University of Sao Paulo, 05508-090, Sao Paulo, SP, Brazil

I. Ledoux-Rak
Laboratoire de Photonique Quantique et Moleculaire, UMR CNRS 8537, Institut d'Alembert, Ecole Normale Superieure de Cachan, 61 av. du President Wilson, 94 235, Cachan, France

1 Introduction

New near-infrared-luminescent materials find numerous applications in the field of optical devices. The longer wavelength emission of lanthanides especially from Er^{3+}, Nd^{3+}, Pr^{3+}, Sm^{3+}, and Yb^{3+} in the near-infrared (NIR) region are gaining an increasing interest due to their potential applications in nonlinear optics [1–5]. For example, Nd^{3+} species find applications in laser systems [6]. Lanthanides such as Pr^{3+} and Er^{3+} prove to be very useful when employed in telecommunication network optical signal amplifiers [7, 8]. Yb^{3+} serves as an efficient sensitizer for other rare earths, which have been used in visible up-conversion lasers and efficient NIR lasers [9]. In addition, the relative transparency of human tissue at around 1000 nm suggests that Yb-based emission could have diagnostic value [10]. The design of efficient NIR luminescence materials based on lanthanide complexes remains an area of active investigation. In continuation of our investigations of lanthanide-doped materials [11–14], we have synthesized $Er_3Al_5O_{12}$ by using the novel combustion process in the present study.

The knowledge of defect centres and the distribution of their energy levels in the band gap of solids is very important in order to elucidate information about the luminescence process of phosphors and to use them in various applications [15–17]. It has been found that trapping centres play an essential role for photo-energy storage in persistent, photo-stimulated, and thermo-stimulated phosphors.

It is well known that the thermally stimulated luminescence process in material is related to the defect centres created owing to ionizing radiation. It has been reported in the literature that in order to minimize the significant influence of performance limiting defects, it is necessary to understand their defect structure [18–20]. The defect centres in a material can be detected and studied well using thermally stimulated luminescence and electron spin resonance methods. However, we found that radiation induced defects in $Er_3Al_5O_{12}$ and their role in thermally stimulated luminescence are receiving little attention. Moreover, the correlation of the TSL peak of $Er_3Al_5O_{12}$ phosphor using the ESR spectra has not been reported so far.

Even though several studies based on rare-earth ions doped alumina (Al_2O_3) and yttrium aluminum garnet ($Y_3Al_5O_{12}$) are available [21–25], studies on $Er_3Al_5O_{12}$ are very rare. Taking these points into account, we have synthesized $Er_3Al_5O_{12}$ by a low-temperature initiated, self-propagating and gas-producing solution combustion method and characterized by using powder X-ray diffraction (PXRD), scanning electron microscopy (SEM) and energy-dispersive analysis of X-ray (EDAX) spectroscopy. Here we report the visible up-conversion and infrared luminescence of $Er_3Al_5O_{12}$ phosphor upon excitation into the $^4I_{11/2}$ level at ∼972/980 nm. In addition, TSL (thermally stimulated luminescence) and ESR (electron spin resonance) studies of $Er_3Al_5O_{12}$ phosphor are also carried out to identify the defect centres.

2 Experimental details

The solution combustion synthesis technique became more popular since it not only saved time and energy but also is very simple to process. Further, the technique is advantageous over the solid-state synthesis process in terms of better compositional homogeneity and purity of the final product and thus was used to synthesize the $Er_3Al_5O_{12}$ phosphor.

Erbium nitrate [1.4182 g, $Er(NO_3)_3{\cdot}5H_2O$, ACROS], aluminum nitrate [2 g $Al(NO_3)_3{\cdot}9H_2O$, ACROS], and glycine [1.0470 g, $C_2H_5NO_2$, Panreac] were used as starting materials and were dissolved in a minimum quantity of deionized water in 300 ml capacity Pyrex dish. The dish was inserted into a preheated furnace maintained at 500°C. In about 5 min. or by the time the set up attained the temperature of furnace, reaction started. The prepared solution undergoes rapid dehydration and foaming followed by decomposition with an evolution of large amount of gaseous by-products. Then, spontaneous ignition occurred and underwent smoldering combustion with enormous swelling, producing foamy and voluminous ash. The combustion was self-sustaining and self-terminated. The entire process lasted 5–8 min. After the completion of the reaction, the dish was removed from the furnace. The products obtained by combustion process were highly fluffy and brown-black masses. This was crushed into a fine powder. The product of the combustion reaction was then given an annealing treatment at 800°C for 5 h in air to remove the thermal stress and impurities during its preparation. After being annealed, the brown-black powder became white and this was used for further characterization.

The phase composition of the synthesized powder was analyzed by XRD using CuKα radiation (Bruker D8 Advance) in the 2θ range of 15° to 80°.

The powders were taken onto a silicon stub with ethanol for their electron microscopic evaluation. After some time the powders were coated with gold and were observed using SEM (S-3400, Hitachi, Japan). Their chemical compositions were analyzed using the EDAX attached to the SEM.

The IR photoluminescence emission spectrum was studied using a Jobin-Yvon TRIAX 180 monochromator with a 150 grooves/mm grating coupled to a multi-channel InGaAs CCD detector. Samples were pumped by a diode (CW) laser operating at ∼980 nm within the power range of 0 to 1 W.

The frequency up-conversion luminescence spectral profile of $Er_3Al_5O_{12}$ phosphor powders were obtained by pumping with a Ti:Sapphire laser (pulse duration ∼15 ns, emission wavelength ∼972 nm). The excitation beam was focused onto the sample with a lens of focal length ∼10 cm. Luminescence was collected in a direction perpendicular to the incident beam and was dispersed by a monochromator (Jobin-Yvon HR460) attached to a Hamamatsu Photonics R955 photomultiplier tube.

For production of the defects, a ^{60}Co gamma source was used for the irradiation of samples. TSL experiments were carried out on a Daybreak 1100 series automated TL reader system with a heating rate of 5°C/s in a nitrogen atmosphere. A Bruker EMX ESR spectrometer operating at X-band frequency with 100 kHz modulation frequency was utilized for Electron Spin Resonance experiments. Diphenyl Picryl Hydrazyl (DPPH) was used for calibrating the g-factors of defect centres. The temperature dependence of the ESR spectra was studied using a Bruker B VT 2000 variable temperature accessory.

3 Results and discussion

3.1 X-ray diffraction

The phase purity and crystal structure of the combustion-synthesized sample were analyzed using the PXRD pattern. Figure 1 shows the PXRD pattern of $Er_3Al_5O_{12}$ powder. From the PXRD pattern, it can be seen clearly that powder shows cubic symmetry with space group la3d. All the reflections in Fig. 1 could be indexed to those of standard

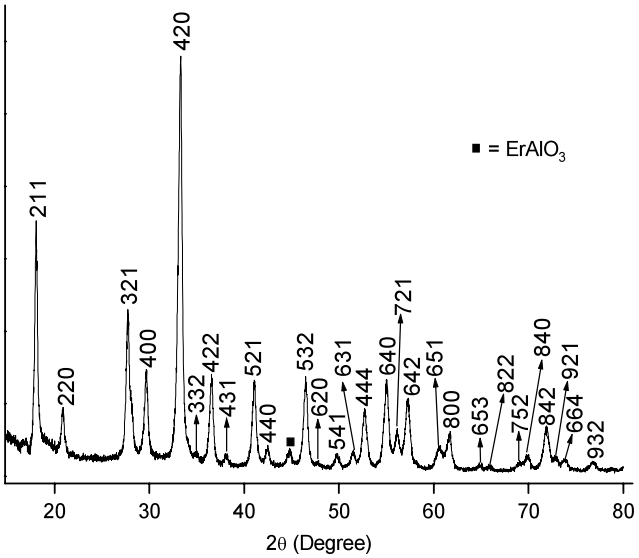

Fig. 1 Powder XRD pattern for $Er_3Al_5O_{12}$ phosphor

cubic $Er_3Al_5O_{12}$ (JCPDS File No. 78-1451) besides one extra weak peak, which might be corresponding to $ErAlO_3$ [JCPDS File No. 24-0396].

3.2 Scanning electron microscopy and EDAX studies

The morphology and chemical composition of $Er_3Al_5O_{12}$ phosphor was characterized by scanning electron microscopy and EDAX (Figs. 2 and 3). Figures 2a, b and c represent SEM images of the powders under various magnifications. SEM micrograph at low magnification, as shown in Fig. 2a, indicates that grains are agglomerated with non-uniform shapes and sizes. A number of voids and pores formed by the escaping gases during combustion can be seen in Fig. 2b, which is a magnified view of Fig. 2a (zone a). Figure 2c which is a magnified view of Fig. 2b (zone b) shows the presence of several small particles within the grains. During the combustion process when the gas was escaping with high pressure, pores are formed with the simultaneous formation of small particles near the pores. The powders obtained from the combustion process contain small particles and many voids and pores of non-uniform shapes and sizes. These entire features are inherent in combustion-derived powders.

Figure 3 shows the EDAX spectrum of $Er_3Al_5O_{12}$ phosphor. The EDAX spectrum confirmed that the phosphor was composed of erbium, aluminum and oxygen elements. Besides these peaks EDAX spectrum shows two additional peaks Au and Si, which are appearing due to coating and substrate respectively. The existence of several erbium peaks in the spectrum has indicated that Er is well distributed with aluminum and oxygen elements and forms the $Er_3Al_5O_{12}$ matrix. In order to achieve an efficient amplification, the homogeneous distribution of Er^{3+} ions in a matrix is essential [26].

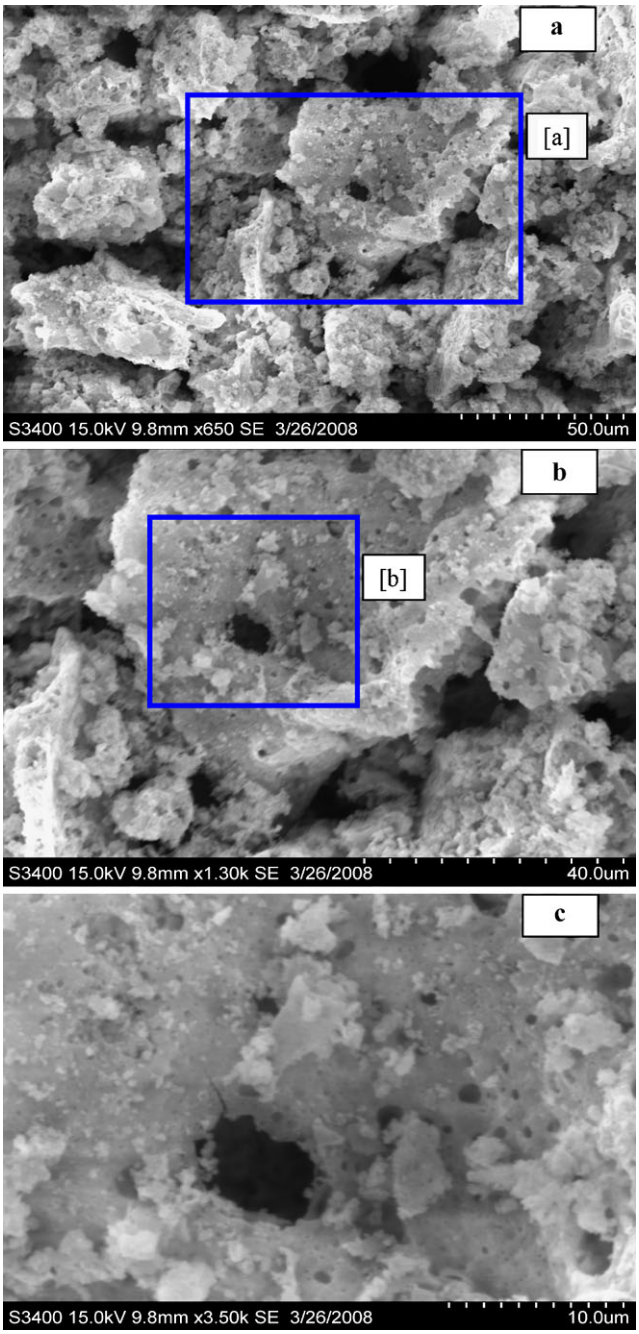

Fig. 2 SEM images of $Er_3Al_5O_{12}$ phosphor

3.3 Up-conversion and IR luminescence of $Er_3Al_5O_{12}$ phosphor

The frequency up-conversion spectral profile from $Er_3Al_5O_{12}$ phosphor powders upon excitation into the $^4I_{11/2}$ level from a Ti-Sapphire laser of nanosecond pulses is presented in Fig. 4. There appear four peaks lying in the violet, green and red regions respectively corresponding to the $^2H_{9/2} \rightarrow {}^4I_{15/2}$; $^2H_{11/2}$, $^4S_{3/2} \rightarrow {}^4I_{15/2}$ and $^4F_{9/2} \rightarrow {}^4I_{15/2}$ transitions. These emissions correspond to the 4f–4f

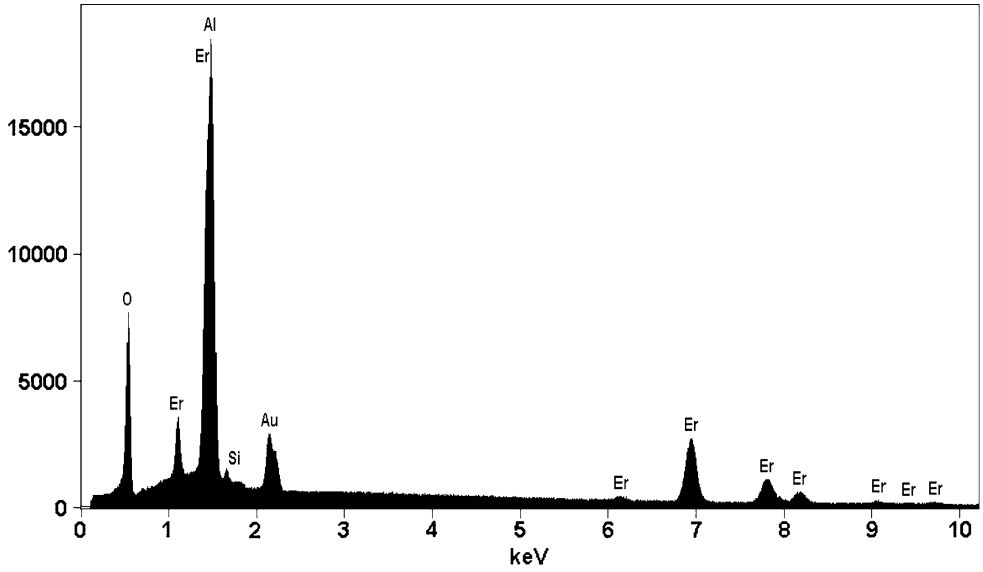

Fig. 3 EDAX spectrum of $Er_3Al_5O_{12}$ phosphor

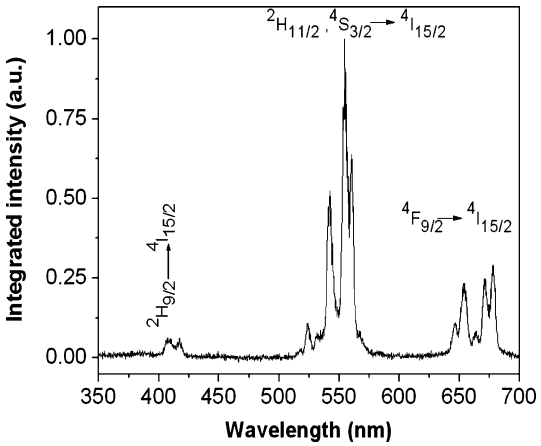

Fig. 4 Up-conversion luminescence of $Er_3Al_5O_{12}$ phosphor. Ti:Sapphire pulsed laser (pulse duration ~15 ns, emission wavelength ~972 nm) was used as an excitation source

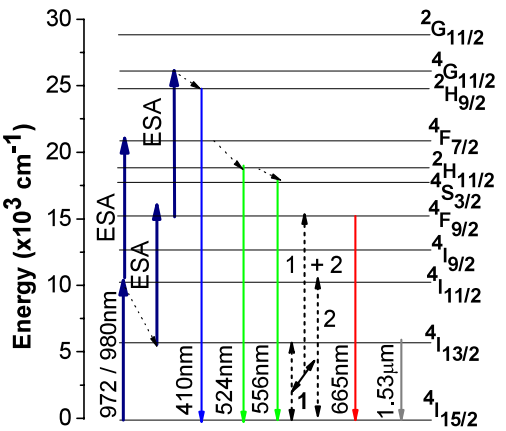

Fig. 5 Energy level diagram of Er^{3+}

transitions of triply ionized erbium ions. An excellent signal to noise ratio is observed showing the high efficiency of the up-conversion process. The Er^{3+} bands positions are in agreement with results reported for other host matrices [27]. The strong frequency up-conversion luminescence appears to the eyes as an intense green colour. The up-conversion luminescence peaks reveal a rather large number of sub peaks due to the strong crystal field effect of the matrix which is responsible for the large stark splitting. The NIR to visible frequency up-conversion may occur via the following two processes viz. excited state absorption (ESA) and energy transfer (ET). The intensity of the up-conversion luminescence peak corresponding to the $^4S_{3/2} \rightarrow {}^4I_{15/2}$ transition is very high compared to the other emission peaks. The frequency up-conversion luminescence intensity in the green and red regions versus laser intensity was found to exhibit an almost quadratic dependence, while the emission at ~410 nm shows a cubic behavior, thereby showing that two and three NIR laser photons are participating and hence responsible for the emissions respectively due to the $^2H_{11/2}$, $^4S_{3/2} \rightarrow {}^4I_{15/2}$, $^4F_{9/2} \rightarrow {}^4I_{15/2}$ and $^2H_{9/2} \rightarrow {}^4I_{15/2}$ transitions. The possible energy level diagram for Er^{3+} ion is shown in Fig. 5. From this figure, it can be visualized that the up-conversion emission peak corresponding to the $^2H_{9/2} \rightarrow {}^4I_{15/2}$ transition is followed by the absorption of the three photons through excited state absorption (ESA). The excitation path way may be the following.

The population in the $^4I_{13/2}$ level is achieved via the ground state absorption of one NIR laser photon followed by multiphonon emission (radiationless transition) from the $^4I_{11/2}$ level. In the second step, a part of the population stored in the $^4I_{13/2}$ level is pumped to the $^4F_{9/2}$ level through ESA. Afterwards, the excited ions are promoted to the $^2H_{9/2}$ level as a consequence of the second ESA process. The energy difference is again waged by the emission of phonons, which can be represented as

(i) $^4I_{15/2}$ + NIR photon $\overset{GSA}{\rightarrow}$ $^4I_{11/2} \rightarrow {}^4I_{13/2}$ + phonons

(ii) $^4I_{13/2}$ + NIR photon $\overset{1st\ ESA}{\rightarrow}$ $^4F_{9/2}$

(iii) $^4F_{9/2}$ + NIR photon $\overset{2nd\ ESA}{\rightarrow}$ $^2H_{9/2}$

The frequency up-conversion luminescence in the green and red region is followed by the non-resonant absorption of two NIR laser photons through ESA (Fig. 5). In the present case the concentration of Er^{3+} ions is high. Therefore the energy transfer between neighboring excited ions could be the most efficient up-conversion mechanism.

The ET process can be explained as follows. Firstly, the ions in the ground ($^4I_{15/2}$) level are excited through the ground state absorption (GSA) $^4I_{15/2} \rightarrow {}^4I_{11/2}$ of NIR laser photon to the $^4I_{11/2}$ level. The energy transfer between a part of pairs of excited ions in the $^4I_{11/2}$ level takes place promoting one ion to the $^4F_{7/2}$ state and de-exciting the second ion back to the ground state. Then, the frequency up-conversion luminescence in the green region corresponding to the $^2H_{11/2} \rightarrow {}^4I_{15/2}$ and $^4S_{3/2} \rightarrow {}^4I_{15/2}$ transition occurs by the emission of multiple phonons from the $^4F_{7/2}$ level to the lower lying ($^2H_{11/2}$, $^4S_{3/2}$) levels. Moreover, the $^4F_{9/2}$ level may also be populated by the effective processes as shown by the dash lines (1 + 2) (see Fig. 5). The mismatch between the intensities of the bands lying in the green region is only due to the non-radiative relaxations from the $^2H_{11/2}$ level to the $^4S_{3/2}$ level. The above facts clarify why the intensity of the emission band due to the $^4S_{3/2} \rightarrow {}^4I_{15/2}$ transition appears much higher compared to other emission bands and the intensity of the emission band peaking at ~410 nm corresponding to the $^2H_{9/2} \rightarrow {}^4I_{15/2}$ transition seems to be less intense with respect to the $^4F_{9/2} \rightarrow {}^4I_{15/2}$ transition.

Figure 6 shows the NIR to IR luminescence from $Er_3Al_5O_{12}$ phosphor powders upon the excitation with a CW (wavelength ~980 nm) laser. There appear three more peaks on either side of the peak, peaking at 1.53 µm. These side bands are the Stark components of the peak corresponding to the $^4I_{13/2} \rightarrow {}^4I_{15/2}$ transition of Er^{3+} ions due to the strong crystal field strength of the $Er_3Al_5O_{12}$ matrix. The variation of IR luminescence peak intensity versus NIR laser intensity shows a linear behavior, which indicates the contribution of one NIR laser photon for the IR emission at 1.53 µm with its FWHM ~30 nm accountable for an eye-safe telecommunication window to occur.

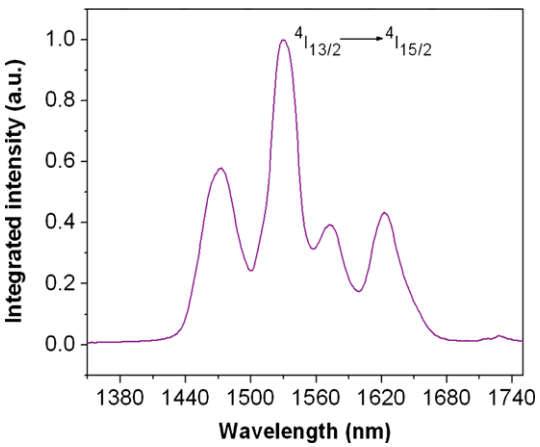

Fig. 6 NIR luminescence of $Er_3Al_5O_{12}$ phosphor under CW excitation at $\lambda_{exi} = 980$ nm

3.4 TSL and ESR of $Er_3Al_5O_{12}$ phosphor

$Er_3Al_5O_{12}$ did not exhibit any glow peaks prior to gamma irradiation. On gamma irradiation with a dose of 5 Gy, $Er_3Al_5O_{12}$ exhibits a single TSL peak at 430°C. The observed glow curve is shown in Fig. 7. The glow curve for the samples was obtained at a heating rate of 5°C/s.

Figure 8 shows the ESR spectrum at room temperature of $Er_3Al_5O_{12}$ phosphor. A single line is observed and the associated center is characterized by an isotropic g-factor equal to 2.0056 and 2 gauss linewidth.

$Er_3Al_5O_{12}$ belongs to rare-earth aluminum garnet family $RE_3Al_5O_{12}$ where RE represents rare-earth atom Lu–Gd

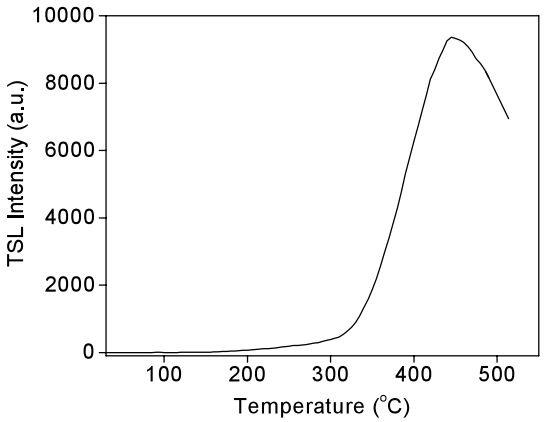

Fig. 7 TSL glow curve of $Er_3Al_5O_{12}$ phosphor (test gamma dose: 5 Gy)

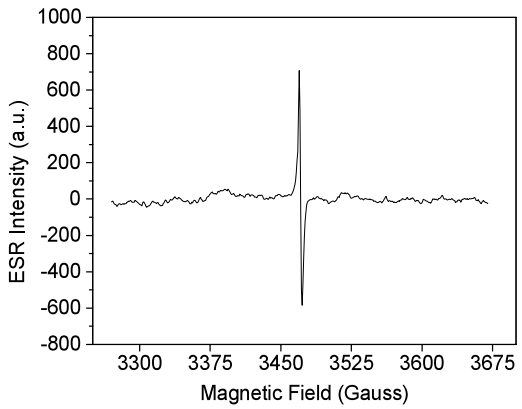

Fig. 8 Room-temperature ESR spectrum of $Er_3Al_5O_{12}$ phosphor

and Y. RE ions in the garnet lattice (space group *Ia3d*) reside on dodecahedral 24c sites, while the Al ions reside on two distinct sites, the octahedral 16a and tetrahedral 24d. Three types of cation vacancy are, therefore, possible in $RE_3Al_5O_{12}$, namely (in Kroger–Vink notation): $(V'''_{Al})_{16a}$, $(V'''_{Al})_{124d}$ and V'''_{RE}. In UV light irradiated $Y_3Al_5O_{12}$ (YAG) garnet at 77 K, Mori [28] has observed in an early ESR study two different defect centres. One of the centres with g-value 1.995 is assumed to be an electron trapped at an oxygen vacancy. On the other hand, the other center with g-value in the range 2.002 to 2.027 is assumed to be the O^- ion. Hayes et al. [29] have pointed out that more than one hole center of the type O^- may be present in the Mori's ESR spectra. These defect centres are unstable at room temperature and have been found to decay around 170 K. Hayes et al. [29] have carried out further studies on X-irradiated YAG at 1.6 K using optical detection of ESR. The observed spectra could be accounted for by postulating three different axial centres. These three centres are associated with the three cation vacancies mentioned above.

Apart from cation vacancies, oxygen vacancies are likely to be present in REAG lattice. Oxygen vacancies have been reported in Ce:YAG by Rotman et al. [30, 31] on the basis of high-temperature transport and luminescence studies. Studies involving the defect structure of isostructural yttrium iron garnet postulate a defect model in YAG based on doubly charged oxygen vacancies. Oxygen vacancies are also likely to be created due to extrinsic defect processes. Based on their diffusion and electro-physical measurements, Neiman et al. [32] have pointed out that oxygen vacancies occur as a consequence of an aluminum deficiency. Intrinsic oxygen vacancies are also likely to occur via Schottky process and this has been predicted on the basis of an atomistic simulation study [33]. Stanek et al. [15] have also utilized such simulation techniques to predict the defect structure that can exist in these rare-earth garnets. Their study has shown that only minimal concentrations of cation vacancies are expected via the relatively high energy Schottky process. Cation vacancies, however, can occur in the lattice as charge compensating defects for impurities. These impurities are introduced extrinsically either through the starting materials used in the preparation of the phosphor or through the synthesis procedures. Further, Stanek et al. have found that oxygen vacancies are also not expected to be a major defect via an intrinsic process. However, oxygen vacancies can occur due to presence of impurities. Therefore, if oxygen and cation vacancies are present in the rare-earth garnets, irradiation will produce O^- ion, F^+ and F centres and the concentrations of such centres are likely to be small due to the reasons mentioned above.

In the context of the theoretical predictions of Stanek et al., we have examined room-temperature irradiated YAG system and the observed spectrum at room temperature is shown in Fig. 9. The spectrum appears to be a superposition of lines arising from three defect centres. One of the ESR lines is broad (center III) with a linewidth of about 45 gauss and a g-factor equal to 2.0049. This center is likely to arise from an O^- ion formed by trapping of a hole on O^{2-} ion adjacent to a cation vacancy. The large linewidth is likely to arise from the interaction of the electronic spin with nearby aluminum ions. It has been mentioned [34] that the charges in oxides must be trapped near double (or more) charged defects in order for the charge to be delocalized and thus allowing it to interact with surrounding nuclei. The ESR lines labelled as I and II in Fig. 9 are due to centres characterized by isotropic g-values equal to 2.0083 and 2.0017 and 8 and 16 gauss linewidth respectively. Centres I and II are most probably the F^+ centres formed by trapping of an electron at an anionic vacancy.

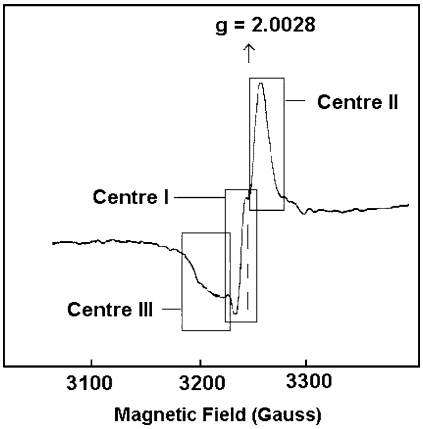

Fig. 9 Room-temperature ESR spectra of $Y_3Al_5O_{12}$ phosphor. Lines labelled as I and II are due to F^+ centres. Center III is due to an O^- ion

The stability of the center observed in $Er_3Al_5O_{12}$ was measured using the pulsed thermal-annealing method. After heating the sample up to a given temperature value where it is maintained for 3 min, it is cooled rapidly down to room temperature for ESR measurements. The thermal-annealing behavior of the center is shown in Fig. 10. It is observed that the center is highly stable and does not show any indication of decay even at 600°C. A probable center which can be formed in $Er_3Al_5O_{12}$ is the F^+ center (an electron trapped at an anion vacancy). Such centres are characterized by a small g-shift, which may be positive or negative, a large linewidth and saturation properties characteristic of an inhomogeneously broadened ESR line. Large linewidths are caused by unresolved hyperfine structure. The defect center formed in $Er_3Al_5O_{12}$ is characterized by a small g-shift and the linewidth is not large. The center also does not exhibit any resolved hyperfine structure. Although the center appears to have the characteristic features of an F^+ center, the high thermal stability precludes us from making an as-

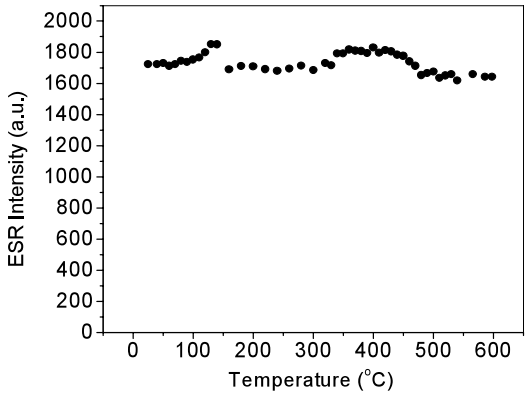

Fig. 10 Thermal-annealing behavior of Center I in $Er_3Al_5O_{12}$ phosphor

signment of this center to F^+ center and it is not clear which species is responsible for the observed ESR spectrum.

The likely centres (O^- ion and F^+ center) originating from cation and anion vacancies are observed in YAG in contrast to $Er_3Al_5O_{12}$. The observations in $Er_3Al_5O_{12}$ are in accordance with the theoretical predictions of Stanek et al. [15]. These observations perhaps can be reconciled with the presence of small concentrations of extrinsic impurities in YAG giving rise to cation and anion vacancies.

TSL studies have shown a high-temperature peak around 430°C. ESR investigations do not indicate any defect center which relates with the TSL peak. It is speculated that F centres are formed in small concentrations in gamma irradiated $Er_3Al_5O_{12}$ (smaller than in the YAG system). At high temperatures (around 350°C), this F center releases an electron in a manner similar to the formation of E_1' center in quartz. In an earlier study, Jani et al. [35] have shown that E_1' centres are not readily formed by room-temperature irradiation. On the other hand, they found that room-temperature irradiation followed by high-temperature annealing leads to an enhanced formation of E_1' centres. A two-step process was suggested for the formation of E_1' center. Initially the room-temperature irradiation converts precursor defects into an intermediate state. High-temperature thermal treatment then converts this state into an E_1' center by transfer of electrons. The precursor defects have been suggested by Jani et al. to be an oxygen vacancy containing two electrons in a singlet state ($S = 0$). This oxygen vacancy with two electrons releases an electron during post irradiation heating resulting in the formation of E_1' center. On the basis of these results in quartz, it is suggested that F^+ centres are forming in $Er_3Al_5O_{12}$ at high temperatures. It is to be noted that the F center also contains two electrons in a singlet state and during heating releases an electron. The released electron could be responsible for the observed TSL glow peak. Thus the F center releases an electron during thermal readout and the released electron can combine with holes trapped elsewhere. The energy released in the electron-hole recombination process is used for the excitation of Er^{3+} ion resulting in the TSL glow peak. It is to be noted that the above mentioned appearance of F^+ center at high temperature was observed in our earlier study of Y_2O_3:Er phosphor [11].

4 Conclusions

We could synthesize $Er_3Al_5O_{12}$ phosphor using a low-temperature, economical solution combustion method. For the phase purity, the fluffy powder obtained after combustion reaction is required to be annealed at 800°C for 5 h. This method proved to be advantageous compared with the other preparation techniques. The $Er_3Al_5O_{12}$ phosphor powders emitted an intense green colour when excited by using a Ti-Sapphire laser (wavelength ~972 nm) of nanosecond pulses at low power. The existence of the efficient two and three photon frequency up-conversion provided a way to identify the current host matrix to be an outstanding candidate for use in photonic devices based on up-converter phosphor. TSL results show the possible presence of a defect center which decays at high temperature. In accordance with the theoretical predictions of Stanek et al., the present study indicates an extremely small concentration of cation and anion vacancies in $Er_3Al_5O_{12}$ phosphor. A defect center which correlates with the observed TSL peak could not be identified based on ESR investigations.

Acknowledgements Vijay Singh is grateful to LPQM, ENS de Cachan (France) for the IR measurements. Mr. Tae-Woo Lee of Research Institute of Advanced Materials, Seoul National University is acknowledged for his assistance in the X-ray diffraction measurements. T.K. Gundu Rao is grateful to FAPESP, Brazil for the research fellowship.

References

1. X. Lu, Z. You, J. Li, Z. Zhu, G. Jia, B. Wu, C. Tu, J. Alloys Compd. **426**, 352 (2006)
2. G. Tripathi, V.K. Rai, S.B. Rai, Opt. Mater. **30**, 201 (2007)
3. L.R. Moorthy, M. Jayasimhadri, A. Radhapathy, R.V.S.S.N. Ravikumar, Mater. Chem. Phys. **93**, 455 (2005)
4. L.-N. Sun, Y. Zhang, J.-B. Yu, C.-Y. Peng, H.-J. Zhang, J. Photochem. Photobiol. A **199**, 57 (2008)
5. G. Boulon, J. Alloys Compd. **451**, 1 (2008)
6. H. Yagi, T. Yanagitani, K. Takaichi, K.-i. Ueda, A.A. Kaminskii, Opt. Mater. **29**, 1258 (2007)
7. B. Je Park, H.S. Seo, J.T. Ahn, Y.G. Choi, D.Y. Jeon, W.J. Chung, J. Lumin. **128**, 1617 (2008)
8. V.A.G. Rivera, E. Rodriguez, E.F. Chillcce, C.L. Cesar, L.C. Barbosa, J. Non-Cryst. Solids **353**, 339 (2007)
9. J.C. Boyer, F. Vetrone, J.A. Capobianco, A. Speghini, M. Bettinelli, Chem. Phys. Lett. **390**, 403 (2004)
10. G.M. Davies, R.J. Aarons, G.R. Motson, J.C. Jeffery, H. Adams, S. Faulkner, M.D. Ward, J. Chem. Soc. Dalton Trans. **8**, 1136 (2004)

11. V. Singh, V.K. Rai, I. Ledoux, S. Watanabe, T.K. Gundu Rao, J.F.D. Chubaci, L. Badie, F. Pelle, S. Ivanova, J. Phys. D, Appl. Phys. **42**, 065104 (2009)
12. V. Singh, D.T. Naidu, R.P.S. Chakradhar, Y.C. Ratnakaram, J.-J. Zhu, M. Soni, Physica B **403**, 3781 (2008)
13. V. Singh, T.K. Gundu Rao, J. Solid State Chem. **181**, 1387 (2008)
14. V. Singh, V.K. Rai, I. Ledoux-Rak, H.-Y. Kwak, Appl. Phys. B **97**, 103 (2009)
15. C.R. Stanek, K.J. McClellan, M.R. Levy, C. Milanese, R.W. Grimes, Nucl. Instrum. Methods Phys. A **579**, 27 (2007)
16. A. Lempicki, R. Bartram, J. Lumin. **81**, 13 (1999)
17. M. Nikl, E. Mihokova, J. Pejchal, A. Vedda, Y. Zorenko, K. Nejezchleb, Phys. Status Solidi B **242**, R119 (2005)
18. D. Robbins, B. Cockayne, B. Lent, C. Duckworth, J. Glasper, Phys. Rev. B **19**, 1254 (1979)
19. S. Rotman, R. Tandon, H. Tuller, J. Appl. Phys. **57**, 1951 (1985)
20. S. Kaczmarek, R. Jablonski, Z. Moroz, I. Pracka, T. Lukasiewicz, Cryst. Res. Technol. **34**, 719 (1999)
21. N. Rakov, G.S. Maciel, J. Lumin. **127**, 703 (2007)
22. H. Wang, M.K. Lei, J. Lumin. **129**, 110 (2009)
23. H. Yang, D.-K. Lee, Y.-S. Kim, Mater. Chem. Phys. **114**, 665 (2009)
24. G. Xia, S. Zhou, J. Zhang, S. Wang, J. Xu, J. Alloys Compd. **421**, 294 (2006)
25. G. Xia, S. Zhou, J. Zhang, S. Wang, Y. Liu, J. Xu, J. Cryst. Growth **283**, 257 (2005)
26. P.G. Kik, A. Polman, Mater. Res. Bull. **23**, 48 (1998)
27. G.H. Dieke, *Spectra and Energy Levels of Rare Earth Ions in Crystals* (Interscience Publishers, New York, 1968)
28. K. Mori, Phys. Status Solidi A **42**, 375 (1977)
29. W. Hayes, M. Yamaga, D.J. Robbins, B. Cockayne, J. Phys. C, Solid State Phys. **13**, L1085 (1980)
30. S.R. Rotman, R.P. Tandon, H.L. Tuller, J. Appl. Phys. **57**, 1951 (1985)
31. S.R. Rotman, C. Warde, J. Appl. Phys. **58**, 522 (1985)
32. A.Y. Neiman, E.V. Tkachenko, V.M. Zhukovskii, Dokl. Akad. Nauk SSSR **240**, 876 (1978)
33. L. Schuh, R. Metselaar, C. Catlow, J. Eur. Ceram. Soc. **7**, 67 (1991)
34. N.Y. Konstantinov, L.V. Karaseva, V.V. Gromov, Dokl. Acad. Nauk SSR **228**, 631 (1980)
35. M.G. Jani, R.B. Bossoli, L.E. Halliburton, Phys. Rev. B **27**, 2285 (1983)